In vivo lung microvasculature visualized in three dimensions using fiber-optic color Doppler optical coherence tomography

Anthony M. D. Lee
Keishi Ohtani
Calum MacAulay
Annette McWilliams
Tawimas Shaipanich
Victor X. D. Yang
Stephen Lam
Pierre Lane

In vivo lung microvasculature visualized in three dimensions using fiber-optic color Doppler optical coherence tomography

Anthony M. D. Lee,[a] **Keishi Ohtani,**[a] **Calum MacAulay,**[a] **Annette McWilliams,**[a] **Tawimas Shaipanich,**[a] **Victor X. D. Yang,**[b] **Stephen Lam,**[a] **and Pierre Lane**[a]

[a]British Columbia Cancer Research Centre, Department of Integrative Oncology—Imaging Unit, Vancouver, British Columbia V5Z 1L3, Canada
[b]Ryerson University, Department of Electrical and Computer Engineering, Biophotonics and Bioengineering Laboratory, Toronto, Ontario M5B 2K3, Canada

Abstract. For the first time, the use of fiber-optic color Doppler optical coherence tomography (CDOCT) to map *in vivo* the three-dimensional (3-D) vascular network of airway segments in human lungs is demonstrated. Visualizing the 3-D vascular network in the lungs may provide new opportunities for detecting and monitoring lung diseases such as asthma, chronic obstructive pulmonary disease, and lung cancer. Our CDOCT instrument employs a rotary fiber-optic probe that provides simultaneous two-dimensional (2-D) real-time structural optical coherence tomography (OCT) and CDOCT imaging at frame rates up to 12.5 frames per second. Controlled pullback of the probe allows 3-D vascular mapping in airway segments up to 50 mm in length in a single acquisition. We demonstrate the ability of CDOCT to map both small and large vessels. In one example, CDOCT imaging allows assignment of a feature in the structural OCT image as a large (~1 mm diameter) blood vessel. In a second example, a smaller vessel (~80 μm diameter) that is indistinguishable in the structural OCT image is fully visualized in 3-D using CDOCT. © *The Authors. Published by SPIE under a Creative Commons Attribution 3.0 Unported License. Distribution or reproduction of this work in whole or in part requires full attribution of the original publication, including its DOI.* [DOI: 10.1117/1.JBO.18.5.050501]

1 Introduction

Vascular remodeling and angiogenesis are important processes in the pathogenesis of many lung diseases such as asthma, chronic obstructive pulmonary disease, and lung cancer.[1] To date, structural information on vascular remodeling in the lung has been primarily investigated in *ex vivo* surgical and postmortem specimens which cannot be used to measure dynamic vasculature parameters such as blood flow speed and directionality. Also, methods that require tissue removal do not permit longitudinal studies to follow vascular changes due to disease progression or response to treatment.

Real-time minimally invasive techniques for mapping the three-dimensional (3-D) vascular network in the airway wall over time may provide new clinical tools for detecting and monitoring lung diseases. Current methods for the visualization of airway vasculature *in vivo* include computed tomography angiography and Doppler ultrasound. However, these methods lack the resolution and sensitivity to detect small vessels. Optical coherence tomography (OCT),[2] has proven to have sufficient resolution for examining tissue morphology and microstructure. Fiber-optic probes have demonstrated *in vivo* endoscopic structural OCT imaging of the lungs.[3–5]

Several techniques based on OCT for visualizing vascular networks have been presented in the literature including several variants of Doppler OCT imaging,[6,7] and structural methods such as speckle variance OCT,[8] and speckle decorrelation.[9] The vast majority of *in vivo* vascular detection techniques have been developed for geometries where access to the region of interest is external to the organism using large-scale galvanometer scanners. Fiber probe-based OCT vascular imaging is considerably more difficult than its galvo-scanned analog because artifacts caused by subject motion are compounded by the additional motion of the fiber probes and their scanning mechanisms. Nonetheless, two-dimensional (2-D) vascular detection inside internal organs using fiber optic based probes using color Doppler optical coherence tomography (CDOCT) has been demonstrated.[10] Here we present the first 3-D CDOCT-generated vascular maps of *in vivo* human airways. In addition to structural information on the tissue morphology, it is hoped that inclusion of vascular maps from CDOCT imaging will provide additional diagnostic capabilities for lung diseases.

2 Methods and Materials

A 50.4 kHz swept source laser (SSOCT-1310, Axsun Technologies Inc., Billerica, Massachusetts) with a polarized output power of 20 mW centered at wavelength $\lambda = 1310$ nm and a bandwidth of ~100 nm (full width half maximum) was coupled 90% sample/10% reference into a single-mode Mach–Zehnder OCT interferometer. The sample arm was connected using a fiber-optic rotary joint (MJP-SAPB, Princetel Inc., Pennington, New Jersey) to a 0.9 mm diameter, rotationally driven, side-looking fiber optic probe (C7 Dragonfly Imaging Catheter, St. Jude Medical Inc., St. Paul, Minnesota). Light exits the probe at approximately 64 deg relative to the tip of the fiber optic probe (i.e., slightly forward looking). For *in vivo* lung imaging, the open-ended probe was inserted into a closed-ended 1.5 mm diameter sheath to prevent direct probe-patient contact and was guided to the imaging location using a bronchoscope. The probe was driven using a custom built motor capable of rotational speeds up to 100 Hz and pullbacks up to 50 mm in length. In this study, the probe was spun at speeds of 6.25 Hz (8064 A-lines/frame) and 12.5 Hz (4032 A-lines/frame). The interference signal was detected using a pair of 75 MHz balanced detectors (PDB420C, Thorlabs-Inc., Newton, New Jersey) using a polarization diversity detection scheme. A high speed digitizer (ATS9350, Alazar Technologies Inc., Pointe-Claire, Quebec) in "k-clock" acquisition mode collected

Address all correspondence to: Anthony Lee, British Columbia Cancer Research Centre, Department of Integrative Oncology—Imaging Unit, Vancouver, British Columbia V5Z 1L3, Canada. Tel: 604-675-8093; Fax: 604-675-8099; E-mail: alee@bccrc.ca

the data. The data was processed to provide live-streaming 2-D structural OCT and CDOCT imaging using custom written data acquisition software. This study was approved by the Research Ethics Board of the University of British Columbia and the British Columbia Cancer Agency. All subjects gave written, informed consent.

The data processing steps to produce a single CDOCT image frame, based on previously reported algorithms[7] are briefly described. The data is collected in the polar domain (r, θ) to generate the structural OCT image and raw CDOCT images using the Kasai velocity estimator:

$$f_{D,(m',n')} = \frac{f_a}{2\pi} \arctan\left\{\frac{\sum_{m=m'}^{m'+M}\sum_{n=n'}^{n'+N-1} I_{m,n+1}Q_{m,n} - Q_{m,n+1}I_{m,n}}{\sum_{m=m'}^{m'+M}\sum_{n=n'}^{n'+N-1} Q_{m,n+1}Q_{m,n} + I_{m,n+1}I_{m,n}}\right\},$$

$$(1)$$

where $f_{D,(m',n')}$ is the Doppler frequency shift of the pixel (m', n'), f_a is the A-scan frequency, and $I_{m,n}$ and $Q_{m,n}$ are the real and imaginary parts of the Fourier-transformed polar pixel (m, n). A high degree of oversampling in the θ-direction is required for reliable CDOCT processing for slower flow velocities deeper into the airway wall because fanning out of the A-lines in our rotational scanning geometry means that adjacent pixels get farther apart at large radii.[11] To improve accuracy, the calculation in Eq. (1) is averaged over M pixels in the radial scan direction, and N pixels in the azimuthal scan direction. For our data sets, we chose $N = 32$, and $M = 8$ as a compromise between color Doppler SNR (which increases with higher values of N and M) and spatial resolution (which decreases with higher values of M and N). The mean velocity $v_{m',n'}$ of the pixel (m', n') is $v_{(m',n')} = \lambda_0 f_{D,(m',n')}/(2n_t \cos \theta)$, where λ_0 is the center wavelength, n_t is the tissue refractive index, and θ is the Doppler angle. Assuming that blood vessels lie parallel to the axis of the airway (i.e., Doppler angle = 64 deg) and $n_t = 1.40$, our nonaliased Doppler velocity measurement range is ± 8.5 mm/s. To reduce Doppler noise, a copy of the structural OCT image is first smoothed using an M by N rectangular kernel. The Doppler image is then masked to include only pixels for which the SNR's of the corresponding smoothed structural OCT image pixels are greater than 2.0. There may be artifact-based Doppler signals following the preceding processing steps that are present due to a combination of three factors: (1) involuntary motion of the subject, (2) in-plane (r, θ) vibrational motion of the rotary probe, and/or (3) out-of-plane (z) pullback motion of the probe. These artifacts are largely removed using a bulk tissue motion correction algorithm that first creates a Doppler velocity histogram for the n'th A-line, $H_v(n)$ from $n-w$ to $n+w$ adjacent A-lines in the θ-dimension (in our case $w = 5$), and specified ROI in the r-dimension. Then, the Doppler velocity of the peak in $H_v(n)$ is subtracted from all Doppler velocities in the n'th A-line. This process is repeated for all A-lines in each frame. The CDOCT and structural OCT images are transformed into Cartesian coordinates to generate cross-sectional views of the airway. Finally, to display the location of the flow regions with respect to the structural image, velocities <1.7 mm/s are masked out prior to overlay on top of the structural image. Raw data sets were reprocessed into movies using MATLAB (Mathworks, Natick, Massachusetts) and 3-D rendered using Amira (Visualization Sciences Group, Burlington, Massachusetts).

3 Results and Discussion

Figure 1 shows structural OCT and CDOCT imaging of a 15 mm long airway segment from a 68-year-old male subject. These images were collected with 8064 A-lines/frame (frame rate = 6.25 Hz) and pullback speed = 1 mm/s (frame pitch = 0.16 mm). Figure 1(a) shows the 3-D rendering of the structural OCT data with a representative 2-D slice shown in Fig. 1(b). Figure 1(c) and 1(d) show the same structural information as Fig. 1(a) and 1(b), respectively, with the CDOCT imaging information overlaid. The color scale for the CDOCT overlay is taken from color Doppler ultrasound convention that dictates that flow towards the probe is shown in shades of red, while flow away from the probe is shown in shades of blue. As light exits the probe slightly forward looking, the color map shows distal-to-proximal blood flow in shades of red, and proximal-to-distal blood flow in shades of blue. A movie of the structural OCT image side by side with the CDOCT overlay of this airway from distal to proximal is presented in Video 1. Figure 1(b) shows a round structure approximately 1 mm in diameter at the 12 o'clock position. The CDOCT image [Fig. 1(d)] clearly shows this structure contains flow, and thus indicates the structure to be a blood vessel that runs alongside the airway. In this case, identifying the architecture of this large vessel using CDOCT imaging alone can be complicated by the fact that the flow within the vessel is pulsatile, and causes the vessel to "blink" on and off in the CDOCT overlay image during the 3-D pullback (Video 1). However, once identified as vasculature using CDOCT imaging, the feature in the structural OCT movie can be used to map the entire vessel. The complete vessel is readily visible as a dark shadow in the 3-D rendering of the airway and is outlined with a dashed red line in Fig. 1(a). This example demonstrates the necessity of using both structural OCT and CDOCT imaging modalities to identify and map
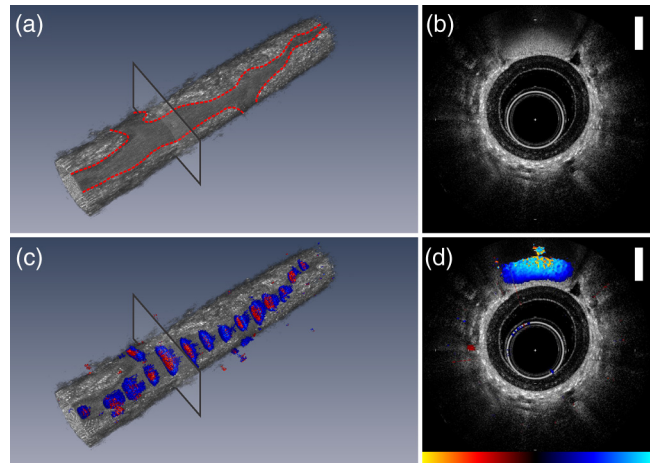
Fig. 1 A 15-mm-long segment of airway from a 68-year-old male subject oriented distal to proximal left to right. (a) Three-dimensional (3-D) rendered structural optical coherence tomography (OCT) volume and (c) color Doppler optical coherence tomography (CDOCT) overlay onto the structural OCT volume of the OCT 3-D-pullback data. (b) Two-dimensional (2-D) cross-sectional structural OCT image and (d) CDOCT overlay on the structural OCT image taken from the locations indicated in (a, c). The scale bars in (b, d) are 0.5 mm. The CDOCT scale bar shown in (d) spans ± 8.5 mm/s. A 2-D structural OCT and CDOCT overlay movie of this airway from distal to proximal is presented in Video 1 (MPG, 5.3 MB) [URL: http://dx.doi.org/10.1117/10.1117/1.JBO.18.5.050501.1].
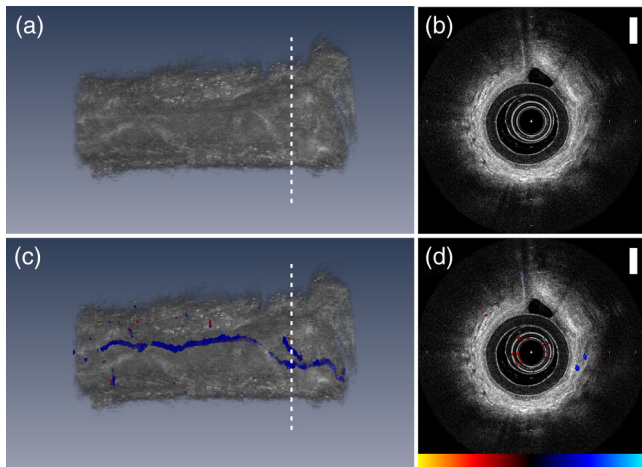
Fig. 2 An 8-mm-long segment of airway from a 52-year-old male subject oriented distal to proximal left to right. Subfigures are presented as in Fig. 1. A 2-D structural OCT and CDOCT overlay movie of this airway from distal to proximal is presented in Video 2 (MPG, 8.6 MB) [URL: http://dx.doi.org/10.1117/10.1117/1.JBO.18.5.050501.2].

vasculature of this nature. The Doppler signal from the vessel is predominantly blue indicating blood flow proximal to distal along the airway. Quantification of velocity in this case requires Doppler phase unwrapping approaches as Doppler aliasing is readily apparent in Video 1.

Figure 2 shows structural OCT and CDOCT imaging of an 8 mm long airway segment from a 52-year-old male subject with subfigures presented as in Fig. 1 with the corresponding movie shown in Video 2. These images were collected with 4032 A-scans/frame (frame rate = 12.5 Hz) and pullback speed 0.6 mm/s (frame pitch = 0.048 mm). In the 3-D rendering shown in Fig. 2(c), a larger, deeper blood vessel has been cropped to reveal the underlying smaller, approximately 80 μm diameter vessel shown. This vessel follows the airway and is joined by another vessel of similar size near the proximal end. The blue color of vessel in CDOCT indicates that flow in this vessel is also proximal to distal along the airway. In this case, the small vessel is continuously visualized by CDOCT in Video 2 as it does not exhibit the same magnitude of pulsatility as the larger vessel seen in F. 1. Unlike the previous airway, there is no obvious feature in the structural OCT images that corresponds to the 80-μm diameter blood vessel. However, CDOCT unequivocally identifies and maps this blood vessel along the entire length of the airway.

Comparing the CDOCT imaging quality between the two airways presented, Video 1 (8064 A-lines/frame) shows fewer radial artifacts due to laser phase instability than Video 2 (4032 A-lines/frame). However, the faster frame rate in Video 2 (12.5 fps) compared to Video 1 (6.25 fps) should mitigate subject motion artifacts more effectively and allows for finer imaging resolution along the airway axis.

In comparison to other OCT vasculature detection modalities, CDOCT is ideally suited for endoscope-guided vasculature detection in the lung. As this implementation of CDOCT only relies on intraframe data processing to extract vasculature, it is less sensitive to ever-present subject and probe motion that can cripple techniques that require frame-to-frame image stability. Rotating fiber optic probes can also be plagued by nonuniform rotational distortion that can complicate inter-frame algorithms even in subject-motion-free environments.

4 Summary

This study demonstrates for the first time 3-D imaging of *in vivo* lung vasculature using fiber-optic CDOCT. For diseases where vascular remodeling and angiogenesis play central roles, 3-D mapping of the lung vasculature may provide important insight into disease detection and diagnosis, following disease progression/regression, and interventional monitoring. In combination with morphological information gleaned from structural OCT imaging, vascular imaging is expected to increase the diagnostic capabilities of lung OCT imaging.

References

1. N. F. Voelkel et al., "Angiogenesis in chronic lung disease," *Chest J.* **131**(3), 874–879 (2007).
2. D. Huang et al., "Optical coherence tomography," *Science* **254**(5035), 1178–1181 (1991).
3. M. Tsuboi et al., "Optical coherence tomography in the diagnosis of bronchial lesions," *Lung Cancer* **49**(3), 387–394 (2005).
4. S. Lam et al., "In vivo optical coherence tomography imaging of preinvasive bronchial lesions," *Clin. Cancer Res.* **14**(7), 2006–2011 (2008).
5. L. P. Hariri et al., "Volumetric optical frequency domain imaging of pulmonary pathology with precise correlation to histopathology," *Chest J.* **143**(1), 64–74 (2013).
6. J. A. Izatt et al., "In vivo bidirectional color Doppler flow imaging of picoliter blood volumes using optical coherence tomography," *Opt. Lett.* **22**(18), 1439–1441 (1997).
7. V. X. D. Yang et al., "High speed, wide velocity dynamic range Doppler optical coherence tomography (Part I): system design, signal processing, and performance," *Opt. Express* **11**(7), 794–809 (2003).
8. A. Mariampillai et al., "Speckle variance detection of microvasculature using swept-source optical coherence tomography," *Opt. Lett.* **33**(13), 1530–1532 (2008).
9. X. Liu et al., "Quantitative transverse flow measurement using optical coherence tomography speckle decorrelation analysis," *Opt. Lett.* **38**(5), 805–807 (2013).
10. B. A. Standish et al., "Doppler optical coherence tomography monitoring of microvascular tissue response during photodynamic therapy in an animal model of Barrett's esophagus," *Gastrointest. Endosc.* **66**(2), 326–333 (2007).
11. C. Sun et al., "In vivo feasibility of endovascular Doppler optical coherence tomography," *Biomed. Opt. Express* **3**(10), 2600–2610 (2012).